Seismic input estimate at Fabriano from scaled and extended sources

Fabio Romanelli[1], Angela Saraò[1], Peter Suhadolc[1], Franco Vaccari[1,2]

Summary

The description of short-period source radiation is of utmost importance in developing techniques for strong motion simulation and prediction. The more common approach considers only the kinematics of rupture and several simplified source models have been used with great success to describe gross features of the source process. In this paper we compute synthetic seismograms using a deterministic approach to simulate the strong motion at the Fabriano recording site for a scaled point source and for a two-dimensional source approximation with a uniform slip model. Our approach has been already applied to simulate the strong ground motions of the 1976 Friuli earthquake (North-East Italy), the 1693 Catania earthquake, and the strongest 1997 Umbria-Marche earthquakes (central Italy).

1. Introduction

One of the basic problems associated with the study of the seismic hazard is the estimate of the seismic ground motion due to an earthquake with a given magnitude at a certain epicentral distance from a site of interest. The optimal solution for such a problem would be the use of a wide database of recorded strong motions where accelerograms with similar source, path and site effects are grouped together. In practice however, such a database is not presently available and will be hardly complete for all earthquake-prone sites also in the future. In fact, the number of recorded signals in most areas of the world is relatively low and the installation of local arrays in high seismicity zones is a too expensive task that requires a long time interval to gather statistically significant data sets. An alternative way of estimating the seismic ground motions associated with a scenario earthquake is based on the computational modelling that incorporates our present knowledge of the seismic source process and of the seismic wave propagation. In such a way synthetic seismograms, to be used as seismic input in a subsequent engineering analysis, can be immediately produced at a very low cost/benefit ratio for the seismic hazard mitigation purpose.

In this paper, using the modal summation technique [e.g. PANZA, 1985; FLORSCH *et al.*, 1991], we estimate the seismic ground motions in the city of Fabriano (Central Italy) for a laterally homogeneous medium. Our approach allows us to accurately calculate synthetic signals that include body and surface waves propagating from different sources and media, taking into account also the effect of local site conditions. To perform the parametric studies needed to characterize the variability of the expected ground motion as function of the source parameters (e.g. focal depth, dip, rake), a simplified model of the seismic source, in the point approximation, is introduced using GUSEV [1983] spectral laws as given by AKI [1987]. However, also kinematic models for a spatially extended source [e.g. PANZA and SUHADOLC, 1987; SARAÒ *et al.*, 1998] can be tackled by our approach. In such a case the generation of seismic waves due to an extended source is obtained by approximating the source with a rectangular plane surface corresponding to the fault plane on which the main rupture process is assumed to occur. Effects of directivity and of the energy release on the fault can be easily modeled.

This study is a contribution to a GNDT project (6A.4) and represents a continuation of the activity began at the end of 1997, concerning the seismic microzonation of Nocera Umbra, Sellano and Fabriano.

2. Synthetic seismograms due to scaled sources

The scenario earthquake chosen for this study is the April 24, 1741 earthquake, a strong historical event whose epicenter has been estimated at approximately 8 km east of Fabriano. The epicentral coordinates and the assumed focal mechanism parameters, a normal fault mechanism that is typical of the studied area, are listed in Tab. I. The coordinates of Fabriano (43.335N, 12.905E) (Fig. 1) have been taken from ISTAT catalogue of the Italian Comuni. The structural model of density and velocities used in the calculations corresponds to the regional model already adopted within GNDT [COSTA *et al.*, 1993] to

(1) Dipartimento di Scienze della Terra, Trieste University, Italy.
(2) INGV, Rome, Italy.

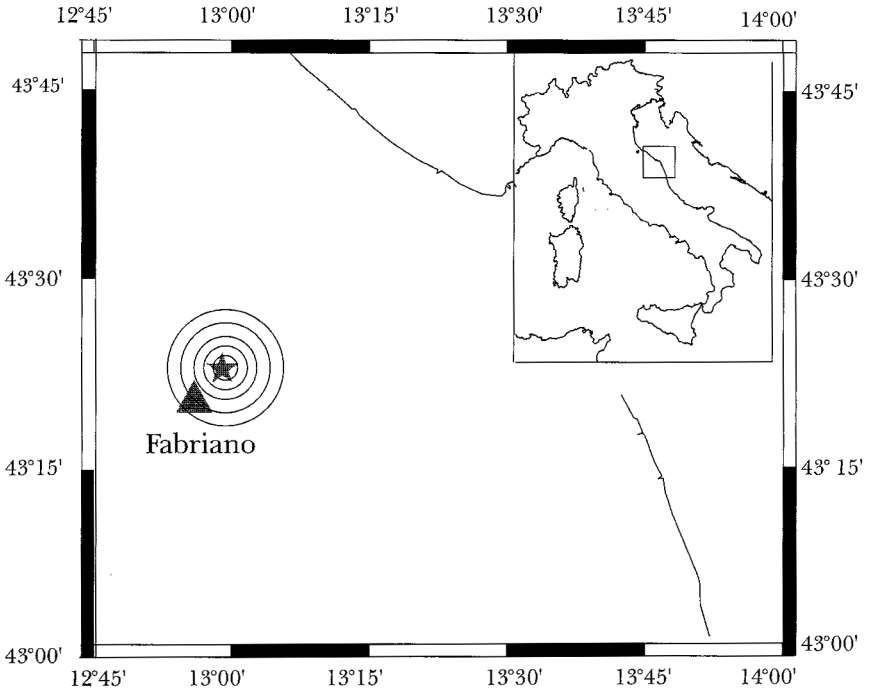

Fig. 1 – Location of Fabriano (triangle) and the 1741 earthquake epicenter (star).
Fig. 1 – Collocazione geografica di Fabriano (triangolo) e dell'epicentro del terremoto del 1741 (stella).

represent the average Umbria-Marche region velocity structure (Fig. 2). We assign to the source a magnitude equal to 6.2 and 6.3, that correspond to a seismic moment of $2.24 \cdot 10^{25}$ Nm and $3.16 \cdot 10^{25}$ Nm respectively, using the GUSEV [1983] spectral laws as given by AKI [1987].

Assuming a double-couple source, we compute synthetic three-component time series in the displacement, velocity and acceleration domains up to 10 Hz, for hypocenters 10, 15 and 20 km deep and for both magnitudes 6.2 and 6.3. In Fig. 3 we show, as an example, the acceleration time series. This first database of 54 synthetic signals, has been further expanded with a parametric study of the ground motion, introducing some possible variations of the dip (20°, 30°, 40°, 50°, 60°) and rake (0°, 45°, 90°, 135°, 180°, 225°, 270°, 315°) angles. For this study we fixed the hypocenter 5.3 km deep (chosen for a subsequent comparison with the results discussed in Section 3), the magnitude (6.3) and the strike angle (150°), obtaining the results shown in Figs. 4 and 5, respectively.

The dataset obtained has been used to quantify the corresponding variability in the frequency domain. The Fourier and response spectra have been computed for the three components of motion, and for the displacement, velocity and acceleration time series. In Fig. 6 we show the average Fourier spectra (6a) and the average response spectra (6b), along with their standard deviation, for the set computed with different dip angles, whereas in Fig. 7a and 7b we plot the curves obtained for the set computed with different rake angles.

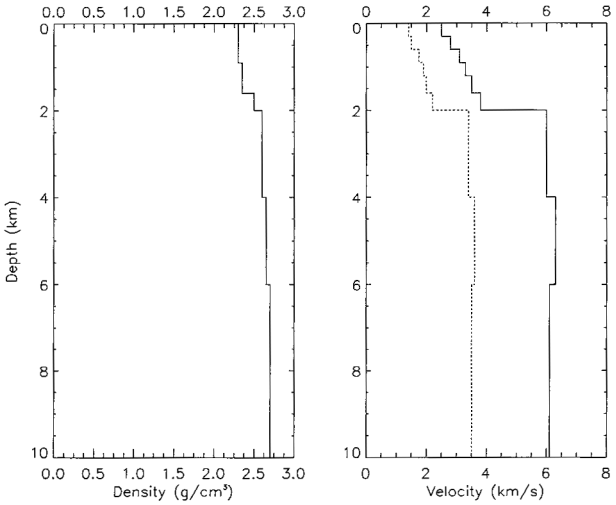

Fig. 2 – Density values and the P-wave (solid line) and S-wave (dashed line) velocities versus depth of the adopted structural model. The corresponding quality factor (not shown), Q, is 100 for S waves and 200 for P waves.
Fig. 2 – Parametri elastici del modello di struttura adottato nei primi 10 km di profondità. Sono riportati i valori di densità e di velocità delle onde P (linea continua) e delle onde S (linea tratteggiata) in funzione della profondità. Il corrispondente valore del fattore di qualità Q (non in figura) è 100 per le onde S e 200 per le onde P.

Tab. I – Parameters of the focal mechanism adopted for the modeled 1741 event.
Tab. I – Parametri del meccanismo focale adottato nella modellazione dell'evento del 1741.

Lat	Lon	Strike	Dip	Rake
43.383°	12.983°	150°	40°	270°

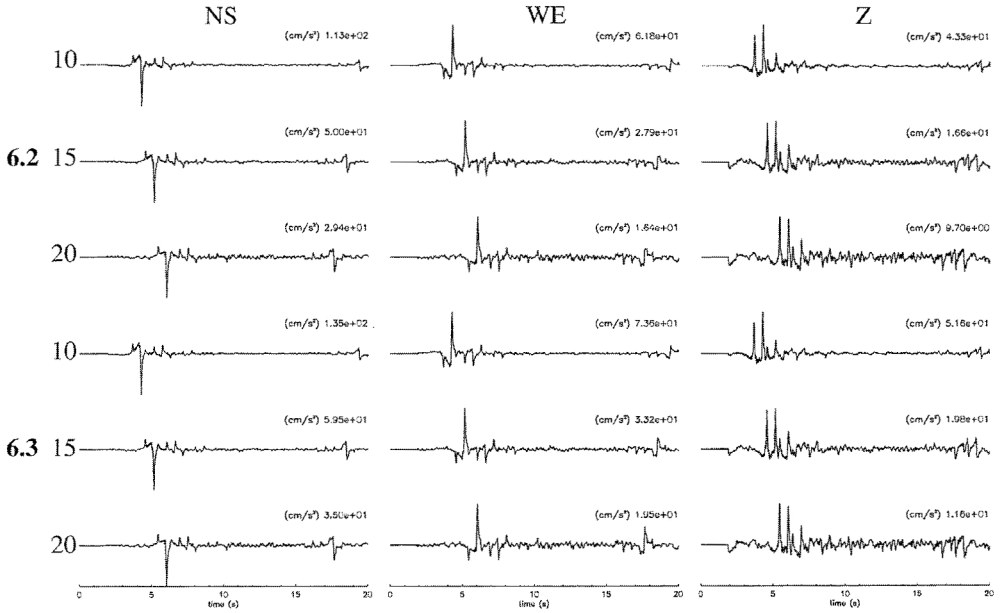

Fig. 3 – Accelerations calculated for the focal mechanism of Tab. I: three components of motion (NS first column, WE second column and Z third column), and for a magnitude equal to 6.2 (first three rows) and 6.3 (last three rows). The peak value (cm/s^2) of each time series is shown near each trace. For each magnitude, the rows correspond to a focal depth equal to 10, 15 and 20 km, respectively.

Fig. 3 – Accelerazioni calcolate per il meccanismo focale di Tab. I: le tre componenti del moto (NS prima colonna, WE seconda colonna, Z terza colonna) sono calcolate per una magnitudo di 6.2 (prime tre righe) e 6.3 (ultime tre righe). Per ogni serie temporale sono riportati i valori di picco (cm/s^2) vicino ad ogni traccia. Per ogni magnitudo, le righe corrispondono alle profondità focali di 10, 15 e 20 km, rispettivamente.

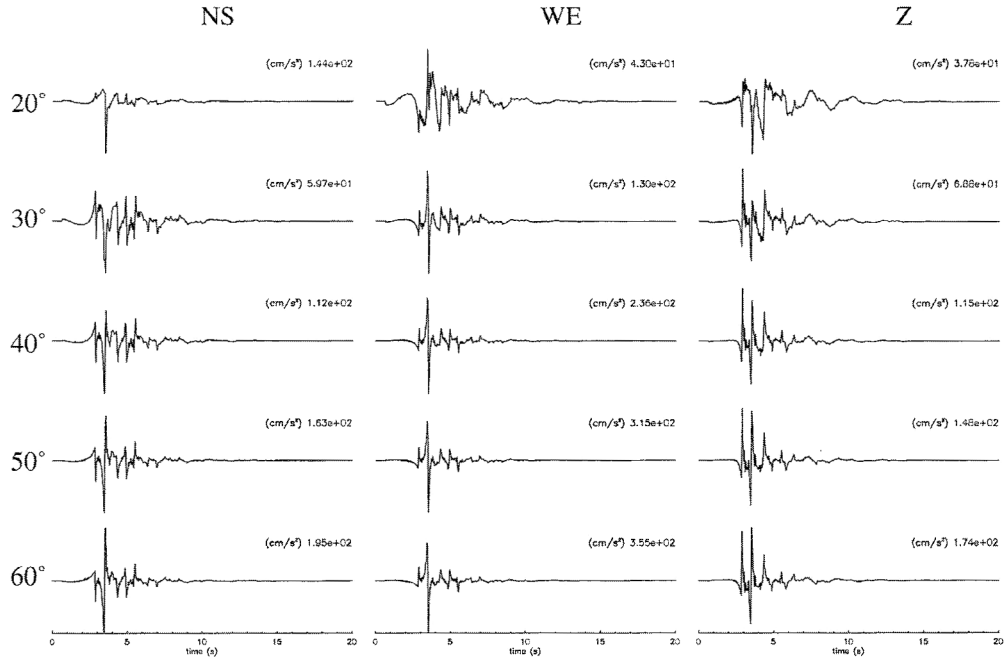

Fig. 4 – Accelerations calculated for the focal mechanism of Tab. I: three components of motion (NS first column, WE second column and Z third column), for a magnitude equal to 6.3 and for a focal depth equal to 5.3 km. The rows correspond to dip angle value equal to 20°, 30°, 40°, 50° and 60°, respectively. The peak value (cm/s^2) of each time series is shown near each trace.

Fig. 4 – Accelerazioni calcolate per il meccanismo focale di Tab. I: le tre componenti del moto (NS prima colonna, WE seconda colonna, Z terza colonna) sono calcolate per una magnitudo di 6.3, per una profondità focale di 5.3 km e per diversi valori di dip. Ogni riga corrisponde ad un valore di dip di 20°, 30°, 40°, 50° e 60°, rispettivamente. Per ogni serie temporale sono riportati i valori di picco (cm/s^2) vicino ad ogni traccia.

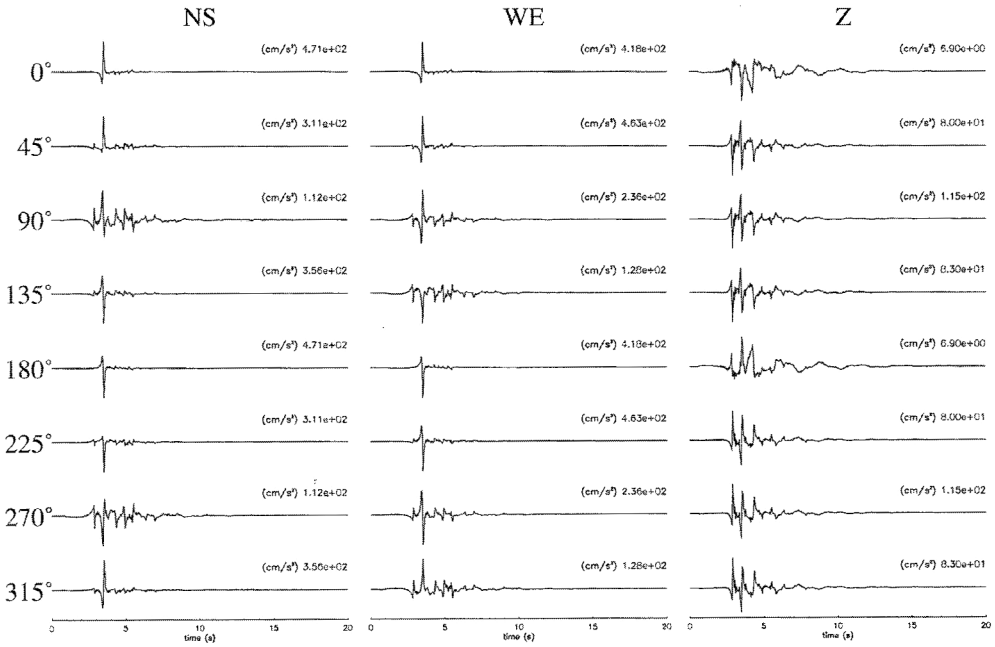

Fig. 5 – Accelerations calculated for the focal mechanism of Tab. I: three components of motion (NS first column, WE second column and Z third column), for a magnitude equal to 6.3 and for a focal depth equal to 5.3 km for different rake values. The rows correspond to rake angle value equal to 0°, 45°, 90°, 135°, 180°, 225°, 270°, 315°, respectively. The peak value (cm/s^2) of each time series is shown near each trace.

Fig. 5 – Accelerazioni calcolate per il meccanismo focale di Tab. I: le tre componenti del moto (NS prima colonna, WE seconda colonna, Z terza colonna) sono calcolate per una magnitudo di 6.3, per una profondità focale di 5.3 km e per diversi valori di rake. Ogni riga corrisponde ad un valore di rake pari a 0°, 45°, 90°, 135°, 180°, 225°, 270°, 315°, rispettivamente. Per ogni serie temporale sono riportati i valori di picco (cm/s^2) vicino ad ogni traccia.

3. Synthetic seismograms due to extended sources

As a further step we compute the synthetic seismograms for an extended source model using a deterministic approach. The seismic source is modeled as a rectangular plane – 10 km × 20 km according to the empirical relationships of WELLS and COPPERSMITH [1994] – discretized into square cells. To avoid aliasing problem 125000 point sources have been considered to model the final time series. At each cell a point source generates a seismogram calculated using the multimodal summation technique [PANZA 1985; PANZA and SUHADOLC, 1987]. The complete signal at each recording station is computed as a sum of point-source seismograms, each one being delayed according to the rupture propagation times on the fault and scaled to include the distribution of energy release on the fault. At the edges of the fault the slip distribution is smoothed by a 2-D cosine tapering function to have a physically realistic slip model [DAS and SUHADOLC, 1996; SARAÒ, 1996; SARAÒ *et al.*, 1998; AOUDIA *et al.*, 1999; 2000]. For modelling the strong motion at the Fabriano bedrock site, we compute three-component accelerograms between 0.1 and 10 Hz assuming a constant energy release model and a total seismic moment of $3.16 \cdot 10^{25}$ Nm. The rupture is a discrete analogue of a Haskell-type model propagating at 75% of the shear wave velocity of the medium (Fig. 2). The top of the fault is 2 km deep, whereas the nucleation point depth is 5.3 km for the rupture models A, B, C and 8.3 km for the rupture models A', B', C' (Fig. 8) respectively. To investigate the effects of directivity, several rupture propagating models are considered: the rupture is bilateral in the model A and A', unilateral from North to South for the models B and B' and from South to North in the models C and C' (Fig. 8). The accelerograms computed for each rupture model, using the same focal mechanism reported in Tab. I, are shown in Fig. 9 and the correspondent spectra are given in Fig. 10. Fig. 11 shows the maximum accelerations, velocities and displacements for each of the rupture models. The maximum values for accelerations and velocities are obtained from an isolated spike of the WE component of model C' (Fig. 9). Neglecting that spike all the WE amplitudes are comparable for each rupture model. Effects of directivity are not very relevant in this case, due to the particular recording site-source geometry. For this case the obtained maximum accelerations are comparable with those retrieved in the scaled point source approximation.

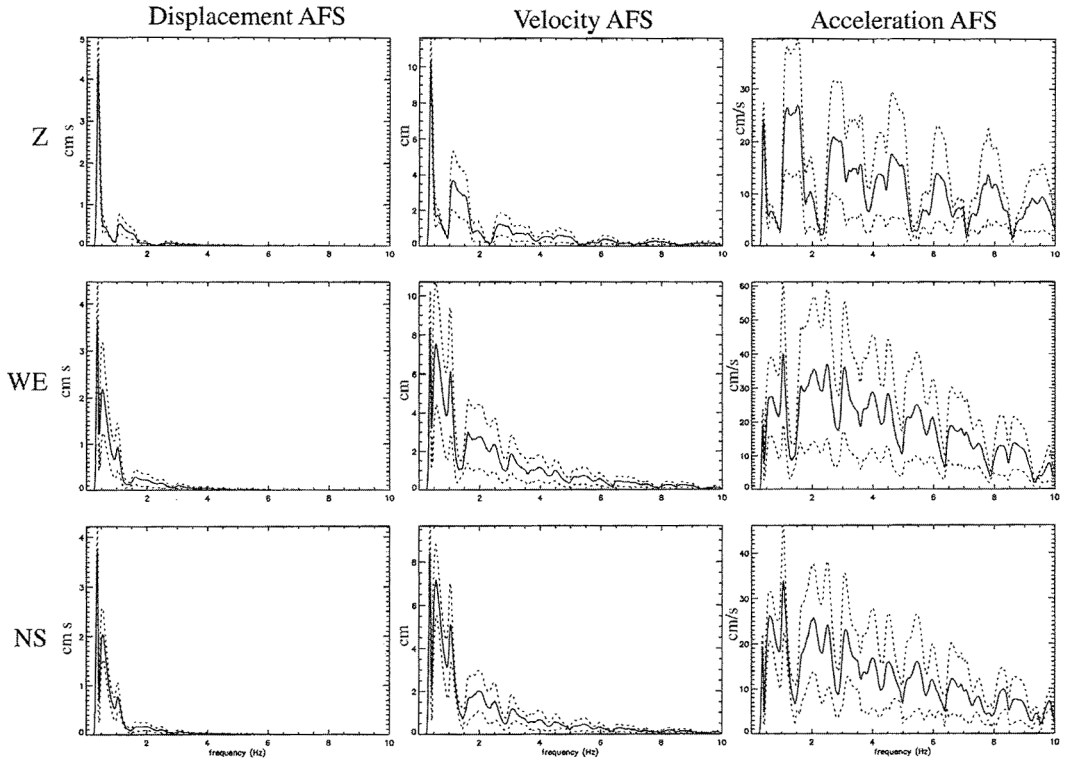

Fig. 6a – Amplitude Fourier Spectra (AFS) calculated for the time series obtained from the variation of the dip angle, for displacement, velocity and acceleration (columns D, V and A, respectively). The rows refer to the components of motion (Z, WE and NS). The average, continuous line, and standard deviation, dashed lines, are shown.

Fig. 6a – Spettri di Fourier in ampiezza (media e deviazione standard), AFS, calcolati per le serie temporali ottenute al variare dell'angolo di dip per spostamento, velocità e accelerazione (colonne D, V e A, rispettivamente). Le righe si riferiscono alle componenti del moto (Z, WE, e NS).

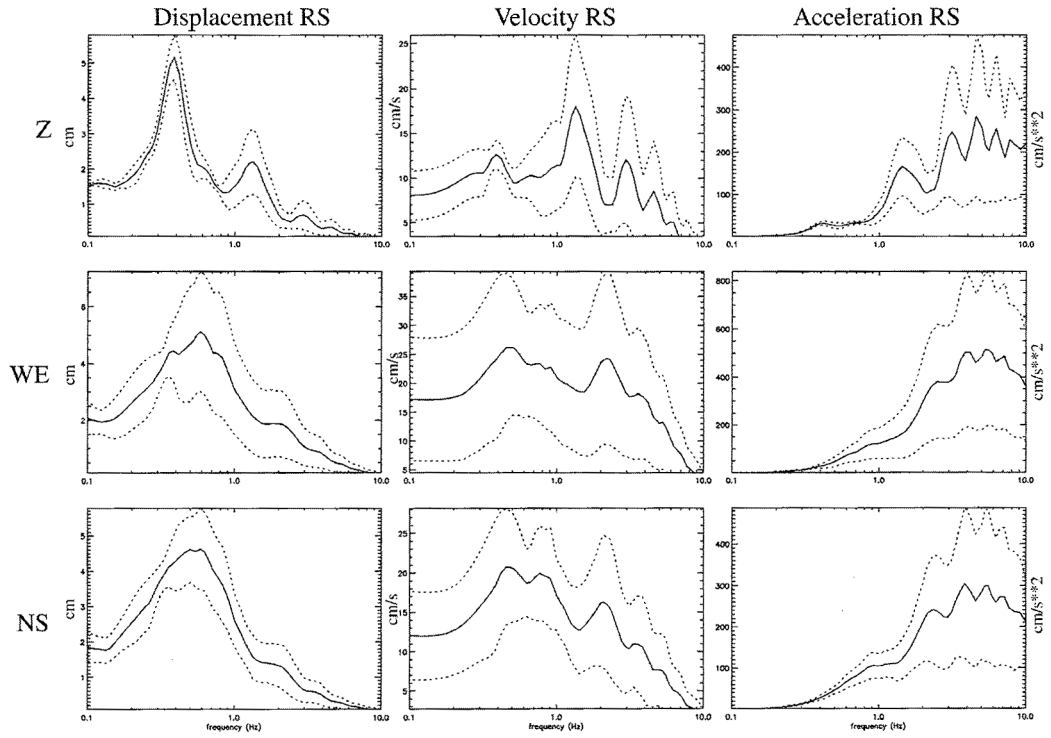

Fig. 6b – Response Spectra (RS), calculated for the time series obtained from the variation of the dip angle, for displacement, velocity and acceleration (columns D, V and A, respectively). The rows refer to the components of motion (Z, WE and NS). The average, continuous line, and standard deviation, dashed lines, are shown.

Fig. 6b – Spettri di risposta (media e deviazione standard), RS, calcolati per le serie temporali ottenute al variare dell'angolo di dip per spostamento, velocità e accelerazione (colonne D, V e A, rispettivamente). Le righe si riferiscono alle componenti del moto (Z, WE, e NS).

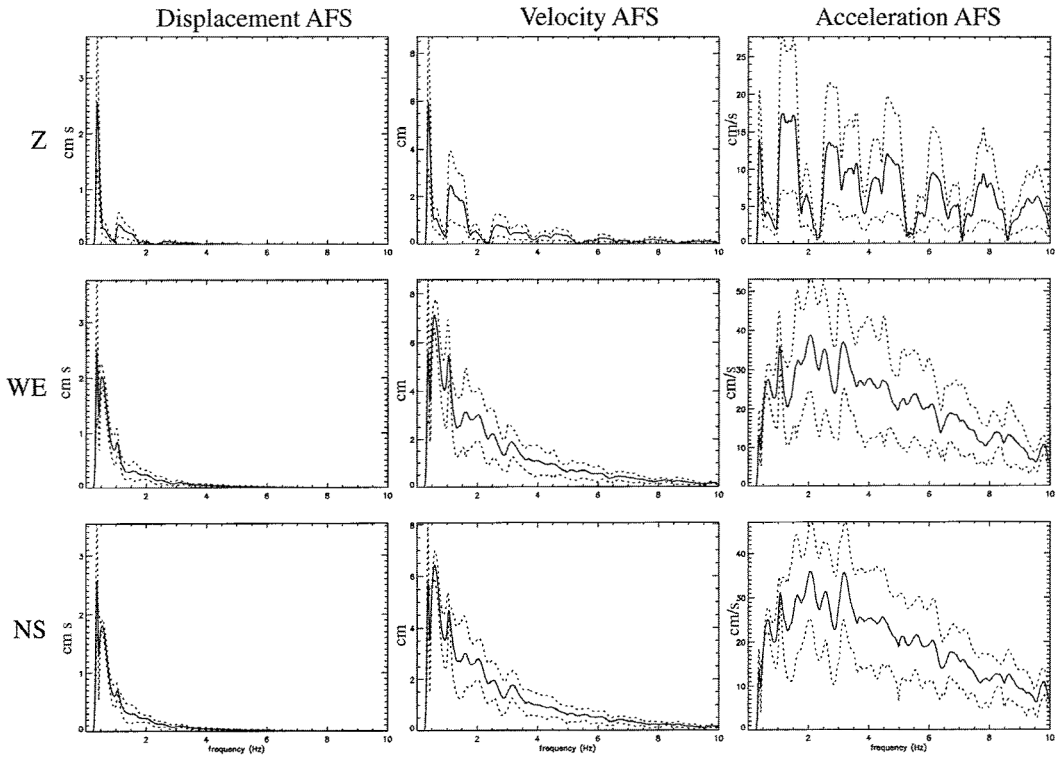

Fig. 7a. Amplitude Fourier Spectra (AFS), calculated for the time series obtained from the variation of the rake angle, for displacement, velocity and acceleration (columns D, V and A, respectively). The rows refer to the components of motion (Z, WE and NS). The average, continuous line, and standard deviation, dashed lines, are shown.

Fig. 7a. Spettri di Fourier in ampiezza (media e deviazione standard), AFS, calcolati per le serie temporali ottenute al variare dell'angolo di rake per spostamento, velocità e accelerazione (colonne D, V e A, rispettivamente). Le righe si riferiscono alle componenti del moto (Z, WE, e NS).

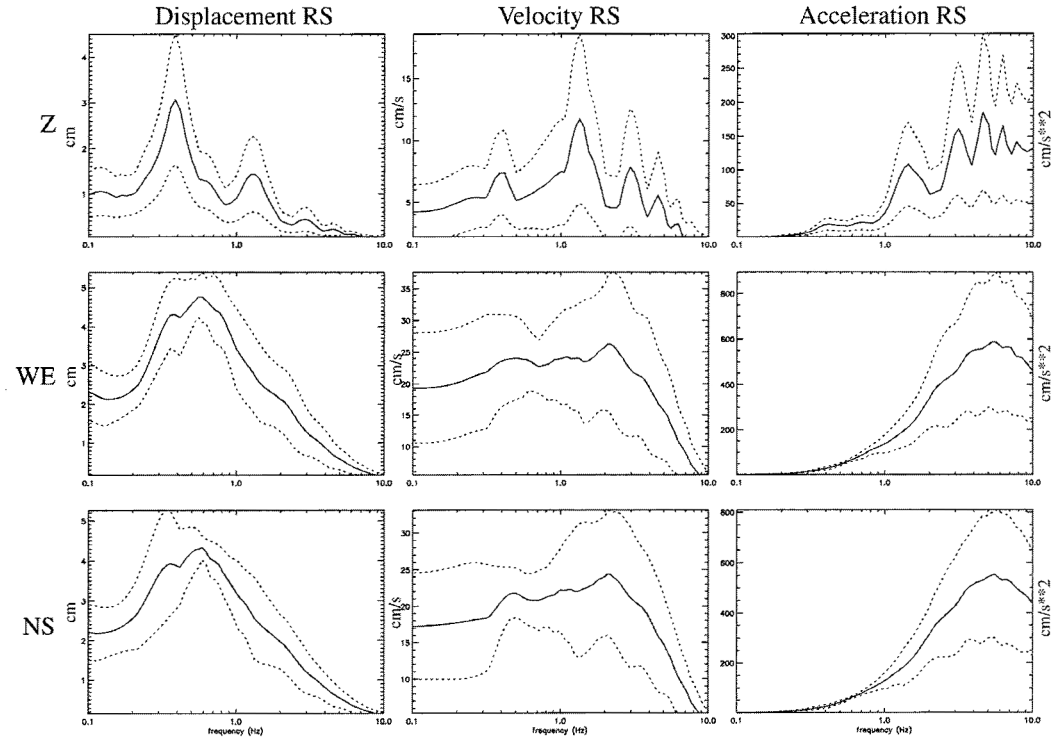

Fig. 7b. Response Spectra (RS), calculated for the time series obtained from the variation of the rake angle, for displacement, velocity and acceleration (columns D, V and A, respectively). The rows refer to the components of motion (Z, WE and NS). The average, continuous line, and standard deviation, dashed lines, are shown.

Fig. 7b. Spettri di risposta (media e deviazione standard), RS, calcolati per le serie temporali ottenute al variare dell'angolo di rake per spostamento, velocità e accelerazione (colonne D, V e A, rispettivamente). Le righe si riferiscono alle componenti del moto (Z, WE, e NS).

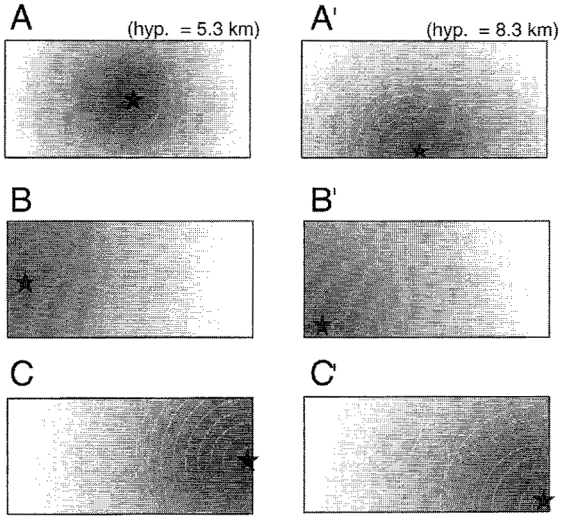

Fig. 8 – Rupture propagation models used in the computation of the accelerograms with an extended source. Rupture nucleation is indicated by the star. The rupture has a constant velocity (75% of S-wave velocity) and propagates bilaterally in A and A' models, unilaterally from North to South in B and B' models, and from South to North in C and C' models.
Fig. 8 – Modelli di propagazione della rottura per la sorgente estesa usata nel calcolo degli accelerogrammi. Il punto di nucleazione della rottura è indicato dalla stella. La rottura si propaga a velocità costante (75% della velocità delle onde S) bilateralmente nei modeli A e A', unilateralmente da Nord a Sud nei modelli B e B', e da Sud a Nord nei modelli C e C'.

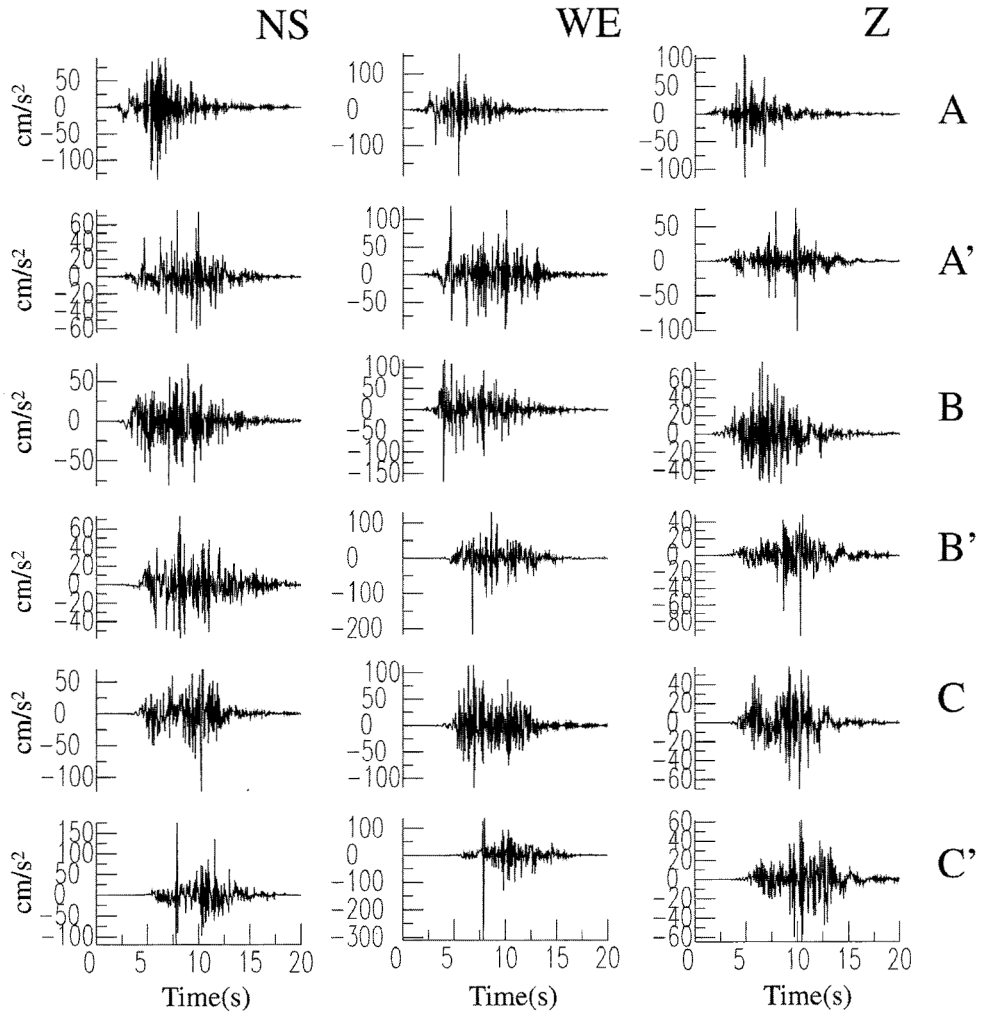

Fig. 9 – Accelerograms computed for the rupture models of Fig. 8.
Fig. 9 – Accelerogrammi calcolati per i modelli di rottura riportati in Fig. 8.

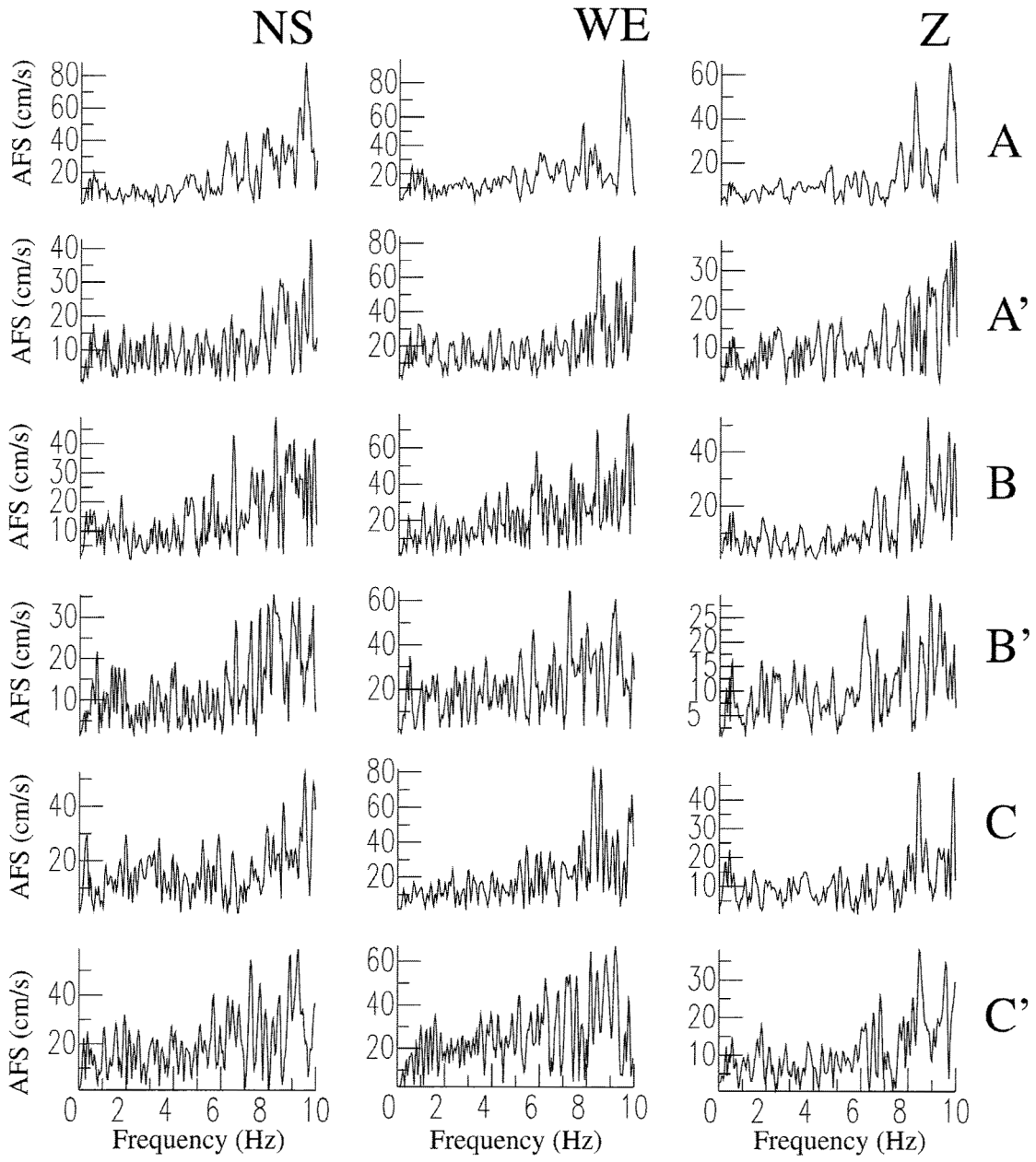

Fig. 10 – Amplitude Fourier Spectra (AFS) calculated for the accelerograms of Fig. 9.
Fig. 10 – Spettri di ampiezza relativi agli accelerogrammi di Fig. 9.

4. Conclusions

We computed synthetic seismograms in the point and extended source approximation in order to determine the expected ground motion variability at the bedrock site of Fabriano. As scenario event we consider the April 24, 1741 earthquake. Our results reveal that when using the scaled point-source approximation and the normal mechanism of Table 1, the maximum acceleration (135 cm/s^2 for the NS component) is obtained for the focal depth of 10 km (Fig. 3). The parametric study performed changing the dip and rake angles (Figs. 4 and 5) of the basic mechanism (Table 1), shows that the maximum values of acceleration are obtained for a dip angle of 60° (355 cm/s^2 for the WE component) and for a strike-slip mechanism (471 cm/s^2 for the NS component), respectively.

When using the extended source approximation, the maximum acceleration value is determined for the WE component of the rupture model where the nucleation is deepest (model C', Figs. 9 and 10). As already noticed, directivity effects seem to be negligible in this case due to the particular position of the site with respect to the fault. The maximum acceleration values obtained with the two source models are the following:

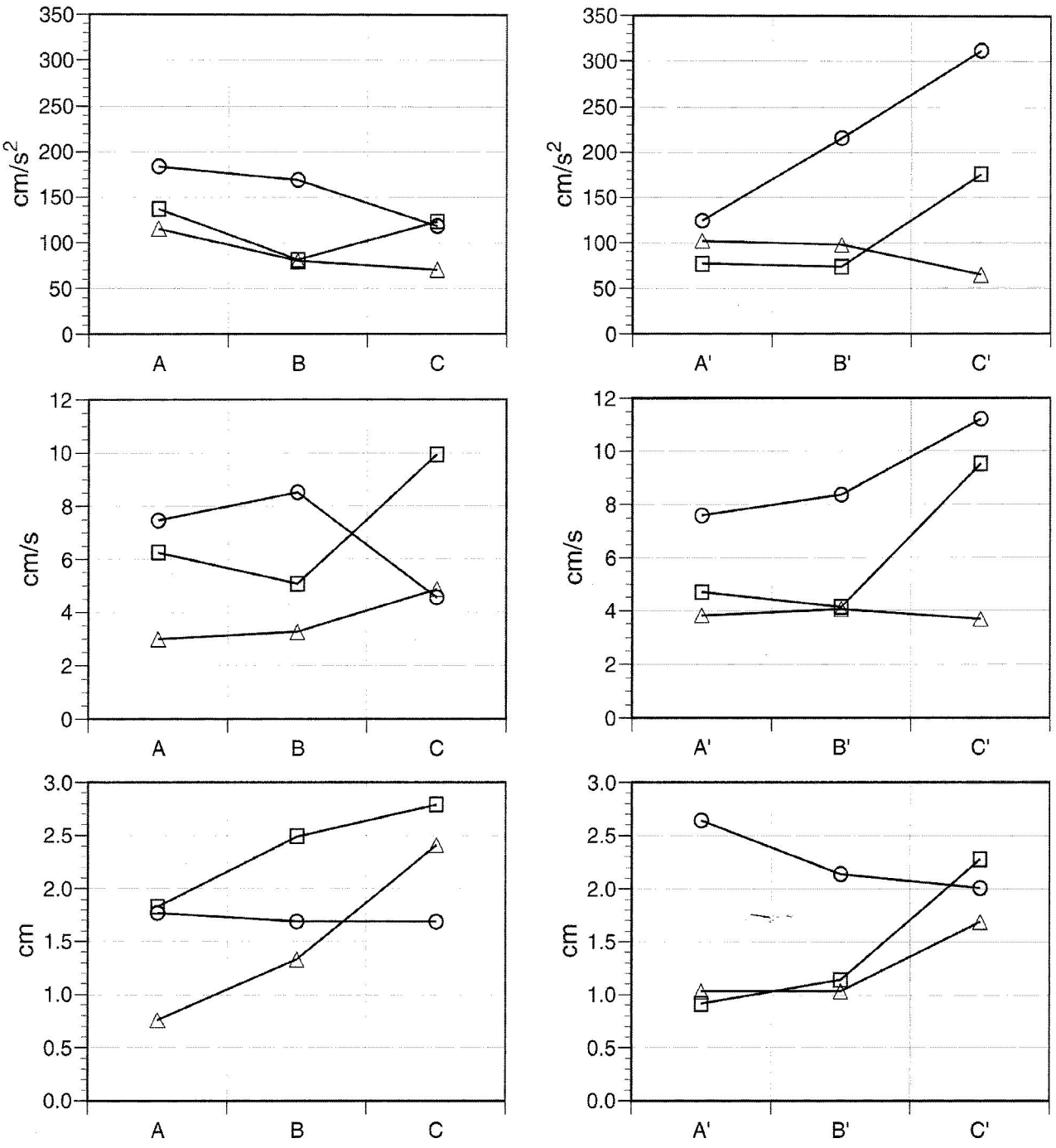

Fig. 11 – Maximum values of accelerations, velocities and displacements reported for the rupture models of Fig. 8. Circles: WE component; squares: NS component; triangles: Z component.
Fig. 11 – Massimi valori di accelerazione, velocità e spostamento riportati per i modelli di rottura di Fig. 8. I cerchietti rappresentano le componenti WE, i quadrati le componenti NS, e i triangoli le componenti Z.

Scaled 236 cm/s^2 for WE 112 cm/s^2 for NS 115 cm/s^2 for Z

Extended 312 cm/s^2 for WE. 176 cm/s^2 for NS 115 cm/s^2 for Z

The comparison shows that the amplitudes calculated for the extended source and the scaled point-source are, for the studied case, in good agreement, with slightly higher values for the horizontal components obtained from the extended source model.

Acknowledgements

This study has been financially supported by CNR 98.03238.PF54 (Gruppo Nazionale per la Difesa dai Terremoti) and MURST Cofinanziamento funds. GMT software [WESSEL & SMITH, 1995] was used for plotting the map of Fig. 1. We acknowledge the two anonymous referees for their useful suggestions.

References

AKI K. (1987) – *Strong motion seismology*. In: M. ERDIK and M. TOKSÖZ (eds.) *Strong ground motion seismology*. NATO ASI Series, Series C: Mathematical and Physical Sciences, D. Reidel Publishing Company, Dordrecht, vol. CCIV, pp. 3-39.

AOUDIA A., CHIMERA G., COSTA G., NUNZIATA C., PANZA G.F., ROMANELLI F., SARAÒ A., SUHADOLC P. and VACCARI F. (1999) – *Modelling of the seismic ground motion of the Umbria-Marche sequence (September 1997)*. Proceedings of the 12th World Conference on Earthquake Engineering, CdRom, paper ID2500, Auckland, New Zealand.

AOUDIA A., SARAÒ A., BUKCHIN B. and SUHADOLC P. (2000) – *The 1976 Friuli (NE Italy) thrust faulting earthquake. A reappraisal 23 years later*. Geophys. Res. Lett, 27, pp. 573-577.

COSTA G., PANZA G.F., SUHADOLC P. and VACCARI F. (1993) – *Zoning of the Italian territory in terms of expected peak ground acceleration derived from complete synthetic seismograms*. In: CASSINIS R., HELBIG K. and PANZA G. F. (eds.) *Geophysical Exploration in Areas of Complex Geology*. II. J. Appl. Geophys., vol. XXX, pp. 149-160.

DAS S. and SUHADOLC P. (1996) – *On the inversion problem for earthquake rupture. The Haskell-type source model*. J. Geophys. Res., 101, pp. 5275-5738.

FLORSCH N., FÄH D., SUHADOLC P., and PANZA G.F. (1991) – *Complete synthetic seismograms for high-frequency multimode SH-Waves*. PAGEOPH , 136, pp. 529-560.

GUSEV A.A. (1983) – *Descriptive statistical model of earthquake source radiation and its application to an estimation of short period strong motion*. Geophys. J. R. Astron. Soc. 74, pp. 787-800.

PANZA G.F. (1985) – *Synthetic seismograms: the Rayleigh waves modal summation*. J. Geophys., 58, pp. 125-145.

PANZA G.F. and SUHADOLC P. (1987) – *Complete strong motion synthetics*. In: B. A. BOLT (ed.) *Seismic Strong Motion Synthetics*, Computational Techniques 4, Academic Press, Orlando, pp. 153-204.

SARAÒ A. (1996) – *Potere risolutivo dei dati nelle inversioni per sorgenti sismiche estese*. PhD Thesis, Dipartimento di Scienze della Terra, Università di Trieste.

SARAÒ A., DAS S. and SUHADOLC P. (1998) – *Effect of non-uniform station coverage on the inversion for seismic moment release history and distribution for a Haskell-type rupture model*. J. Seism., 2, pp. 1-25.

WELLS D.L. and COPPERSMITH K.J. (1994) – *New empirical relationships among magnitude, rupture length, rupture width, rupture area, and surface displacement*. Bull. of Seism. Soc. Am., 4, pp. 974-1002.

WESSEL P. and SMITH W.H.F. (1995) – *New version of the Generic Mapping Tool*. EOS, Trans. Am. Geophys. Union, 76, pp. 329.

Stima dell'input sismico a Fabriano calcolato con sorgenti sismiche scalate ed estese

Sommario

La descrizione della radiazione a corto periodo dalla sorgente è fondamentale per sviluppare tecniche di simulazione e predizione del moto forte del suolo. L'approccio più comune considera solo la cinematica della rottura ed alcuni modelli semplificati sono stati impiegati con grande successo per descrivere gli aspetti principali del processo fisico alla sorgente. In questo articolo simuliamo, con un approccio deterministico, il forte scuotimento del suolo a Fabriano utlizzando sia una sorgente puntiforme scalata che una sorgente bidimensionale con un modello a slip uniforme. Il nostro metodo è stato già applicato per simulare il forte scuotimento del suolo per il terremoto del Friuli del 1976, per il terremoto di Catania del 1693 e per i più forti eventi del 1997 in Umbria-Marche.